

The presence of intermediate-mass black holes in globular clusters and its connection with extreme horizontal branch stars

P. Miocchi*

INAF, Osservatorio Astronomico di Teramo, via M. Maggini, Teramo I-64100, Italy.

Dipartimento di Fisica, Università di Roma “La Sapienza”, P.le A. Moro, 5, Roma I-00185, Italy.

Accepted ?????. Received ????; in original form ????.

ABSTRACT

By means of a multimass isotropic and spherical model including self-consistently a central intermediate-mass black hole (IMBH), the influence of this object on the morphological and physical properties of globular clusters is investigated in this paper. Confirming recent numerical studies, it is found that a cluster (with mass M) hosting an IMBH (with mass M_\bullet) shows, outside the black hole gravitational influence region, a core-like profile resembling a King profile with concentration $c < 2$, though with a slightly steeper behaviour in the core region. In particular, the core logarithmic slope is $s \lesssim 0.25$ for reasonably low IMBH masses ($M_\bullet \lesssim 10^{-2}M$), while c decreases monotonically with M_\bullet . Completely power-law density profiles (similar to, e.g., that of collapsed clusters) are admitted only in the presence of a black hole with an unrealistic $M_\bullet > M$. The mass range estimate $12s - 4.8 < \log(M_\bullet/M) < -1.1c - 0.69$, depending on morphological parameters, is deduced considering a wide grid of models. Applying this estimate to a set of 39 globular clusters (including G1, in M31), it is found that NGC 2808, NGC 6388, M80, M13, M62 and M54 probably host an IMBH. For them, the scaling laws $M_\bullet \sim 0.02(M/M_\odot)^{0.8} M_\odot$ and $M_\bullet \sim 100(\sigma_{\text{obs}}/\text{km s}^{-1})^{0.9} M_\odot$, are identified from weighted least-squares fit. An important result of this ‘collective’ study is that a strong correlation exists between the presence of an extreme blue horizontal branch (HB) and the presence of an IMBH, at a statistically significant level of confidence (> 90 percent). In particular, the presence of a central IMBH could explain why extreme HB stars are observed in M13 and NGC 6388, but not in M3 and 47 Tuc where this object is likely absent according to our analysis.

Key words: black hole physics – stellar dynamics – methods: analytical – methods: numerical – galaxies: kinematics and dynamics – globular clusters: general – stars: horizontal branch

1 INTRODUCTION

The presence and origin of intermediate-mass black holes (IMBHs) at the centre of globular clusters, are still under debate inside the astrophysical community (see the recent general reviews in van der Marel 2004; Rasio et al. 2006). There are essentially two main formation theories: they could be Population III stellar remnants (see, e.g., Madau & Rees 2001) or could form in a runaway merging of young stars in suffi-

ciently dense clusters (e.g., Portegies Zwart et al. 2004; Gürkan, Freitag, & Rasio 2004; Freitag et al. 2006b).

The IMBHs existence is suggested primarily by an argument of plausibility: they would fill the ‘embarrassing’ gap between stellar black holes (with mass $M_\bullet \lesssim 10 M_\odot$) and super-massive black holes (BH) (having $M_\bullet \sim 10^4\text{--}10^9 M_\odot$) whose presence is, by now, practically ascertained in the nucleus of most galaxies (e.g., Kormendy 2004; Richstone 2004; Ferrarese & Ford 2005, for recent reviews). Exploiting the accurate kinematics measures of gas and stars in nearby galaxies, important correlations between the mass of super-massive BHs and various global properties of their hosting galaxy have

* E-mail: miocchi@uniroma1.it

been deduced (Ferrarese & Ford 2005). For instance, extrapolating the Magorrian et al. (1998) relation $-M_{\bullet} \sim 10^{-3}$ times the mass of the host system – to globular clusters, these would contain BHs with an intermediate mass $M_{\bullet} \sim 10^3\text{--}10^4$, which their denomination comes from.

Indirect observational evidences come from the detection of ultra-luminous X-ray sources radiating at super-Eddington luminosity ($> 10^{39}$ erg s $^{-1}$) and thought to originate from matter infall on BHs considerably more massive than stellar BHs (see Fabbiano 2006, for a review on this subject). In globular clusters, however, direct kinematic observations are seriously obstructed by crowding and by the relatively small number of stars inside the BH gravitational influence region (hereafter BHIR), which cannot be well resolved in many cases. Thus, so far, only very few clusters have been the object of accurate kinematic studies so as to infer about the possible presence of massive objects in the central regions.

We just remind the cases of the core-collapsed M15 (Gerssen et al. 2002, 2003; McNamara, Harrison & Anderson 2003) and 47 Tuc, in which such a presence the latest observational data (van den Bosch et al. 2006 and McLaughlin et al. 2006, respectively) do not confirm yet, and the highly concentrated and massive cluster G1 (in M31), where a central $\sim 2 \times 10^4 M_{\odot}$ IMBH has been claimed to reside (see Gebhardt, Rich, & Ho 2002, 2005), while a very recent deep photometric analysis of the core region of ω Cen seems to be consistent with an IMBH with mass $\sim 10^4 M_{\odot}$ (Noyola et al. 2007). Note, however, that for both M15 and G1, direct and accurate N -body simulations reproduce the observed mass-to-light ratio without the need of an IMBH (Baumgardt et al. 2003a,b). Other, less direct, insights can be gained from the time behaviour of the period of millisecond pulsars sited in clusters central region, which permits to deduce the local acceleration. This occurs in the intriguing case of NGC 6752 where there are indications of the existence of an underluminous and compact component with mass $\sim 10^3 M_{\odot}$ (Ferraro et al. 2003; Colpi et al. 2005, and references therein).

It is interesting to note that the above-mentioned individual studies concerned globular clusters that are supposed to host IMBH because of their (present) high central density and (presently) high rate of stellar collisions in their compact cores. Most of them are core-collapsed clusters, indeed. Nevertheless, present conditions may be drastically different from those at the early epochs of clusters life. More importantly, as firstly argued by Baumgardt, Makino, & Hut (2005), their dynamical status could be even inconsistent with the long-term effects that a IMBH actually produces on the cluster internal evolution. Using collisional N -body simulations, Baumgardt et al. found that the high stellar density in the vicinity of the central IMBH enhances the rate of close encounters that, in turn, induces a rapid expansion of the central region, giving rise to a medium-concentration, King-like profile, whose features are almost independent of the BH mass. They argued that an observable fingerprint of the IMBH presence is just a slight slope of the density in the core region, thus suggesting as probable candidates clusters hosting IMBH, those having a surface

brightness logarithmic slope ~ -0.2 in the core (while the typical projected profile of core-collapsed systems goes like r^{-1}).

Similar conclusions have been recently reached by Trenti et al. (2007) who conducted direct N -body experiments of clusters with IMBHs and realistic fractions of primordial binaries: the expansion of the core is even stronger and the formation of the density cusp is confined in the immediate vicinity of the BH. This leads to density profiles with a core to half-mass radius ratio significantly higher than when the IMBH is absent (Trenti 2006). All these studies are telling us that a IMBH represents a ‘heat’ source in the central region, acting in a way similar to hardening binaries in contrasting gravothermal collapse (see also Heggie & Hut 2003).

However, besides these global morphological hints, other fingerprints of the IMBH presence could be revealed. As known, one of the most important effect of the gravitational influence of the IMBH on the surrounding stars, is the tidal erosion and disruption they undergo during close passages (see, e.g., Frank & Rees 1976; Amaro-Seoane, Freitag & Spurzem 2004; Baumgardt, Makino, & Ebisuzaki 2004a; Freitag, Amaro-Seoane & Kalogera 2006a; Baumgardt et al. 2006). Apart from complete disaggregation, this may lead to a loss of envelope mass of passing-by giants. The mass loss from stellar outer layers is also one of the possible explanation for the not yet ascertained origin of ‘blue subdwarfs’ – also called extreme horizontal branch stars, see Rich et al. 1997 and, for a review on this subject in the context of dense galactic nuclei environment, also Alexander 2005, section 3.4). These are stars heavier and bluer than turn-off stars, which are located at the lower-left end of the horizontal branch (HB), in the region of the color-magnitude diagram referred to as extreme HB (hereafter EHB; see the discussion in Meylan & Heggie 1997, sect. 9.7, and the recent review in Catelan 2007).

Given the cuspy behaviour of the stellar density in the BHIR and the relatively high ratio between M_{\bullet} and the single stellar mass, it is reasonable to expect that this mechanism of blue subdwarfs formation is significantly enhanced by the presence of the IMBH. Thus, the possibility to find some connection between such a presence and that of an abundant population of EHB stars naturally emerges and, to our knowledge, has never been explored so far. This is one of the aim of the present paper.

While the investigation of the dynamical evolution of a cluster harbouring a massive compact object is still at the beginning – because of the recent development of sufficiently advanced computational tools – the study of the stellar phase-space distribution function (DF) around a massive BH in the quasi-steady regime is a classical subject in Stellar Dynamics tackled by several authors since the early 70s (Peebles 1972; Bahcall & Wolf 1976; Shapiro & Lightman 1976; Lightman & Shapiro 1977; Cohn & Kulsrud 1978). If a time much longer than the cluster relaxation time is passed since the BH formation and accretion, dynamical and ‘thermal’ equilibrium can take place and a Maxwellian DF $\sim \exp(-E/\sigma^2)$, with E the total energy and σ a velocity param-

ter, should be established. Nevertheless, close enough to the compact object, stars are either disrupted, because of the strong tidal interaction, or swallowed by the BH, thus generating an outward flux of positive energy that, in stationary conditions, must be constant and uniform through the central region. This precludes the Maxwellian distribution being valid in the BH vicinity. Simple scaling arguments (Binney & Tremaine 1987, section 8.4.7) or treatments based on the ‘heat-transfer’ equation (Freitag et al. 2006b, section 2.2) show, indeed, that a realistic space density behaviour is $\sim r^{-7/4}$.

Such a power-law density (or ‘cusp’) corresponds to a DF $\sim (-E)^{1/4}$, as was first found, through approximate solutions of the Fokker-Planck equation, by Bahcall & Wolf (1976) (hereafter BW76) and more recently confirmed with the help of more accurate methods including relaxation effects, such as: Monte-Carlo codes (Shapiro 1985; Freitag & Benz 2002), gas-dynamical methods (Amaro-Seoane et al. 2004) and direct N -body simulations (Baumgardt et al. 2004a; Preto et al. 2004). However, equilibrium self-consistent models of stellar systems including massive BHs are not so numerous. We just mention the Gerssen et al. (2002) paper on M15 employing spherical non-parametric models and the papers by van den Bosch et al. (2006) and van de Ven et al. (2006), in which axisymmetric models of, respectively, M15 and ω Cen are generated to infer the radial behaviour of the M/L ratio, by means of a generalization of the Schwarzschild (1979) orbit superposition method. A further generalization of this technique has been also recently presented in Capuzzo Dolcetta et al. (2007) to model triaxial galaxies with dark matter and a central density cusp. It is worth noting, finally, that McLaughlin et al. (2006), in order to derive hints about the presence of an IMBH in 47 Tuc, applied a simple single-mass and isotropic King model, even if in a not fully self-consistent way.

In the present study, a self-consistent parametric model is constructed and used to estimate the mass of possible IMBHs in clusters and their influence on the cluster density profile, as well as on the presence of EHB stars. It basically consists of a multimass King model appropriately extended to incorporate the BW76 DF inside the BHIR. The model is spherical, isotropic (in the present version) and relatively easy to construct and use. Its multimass nature makes straightforward the inclusion of central energy equipartition, which is suggested to play a non-negligible role in the presence of a massive BH, too (Bahcall & Wolf 1977; Murphy, Cohn, & Durisen 1991; Baumgardt, Makino, & Ebisuzaki 2004b; Freitag et al. 2006b; Hopman & Alexander 2006).

The model will be described in section 2, while in section 3 the observable features of the generated surface brightness and velocity dispersion profiles will be illustrated, also with respect to the debated structural properties of clusters hosting IMBH. Then, in section 4, the model will be employed to deduce the mass of possible IMBHs from the central density profiles provided by the recent Noyola & Gebhardt (2006) (hereafter NG06) analysis of WFPC2 *Hubble Space Telescope* (HST) observations of 38 galactic globulars (G1 in M31 is considered as well). In section 5, finally, the connection between the

existence of IMBHs and the presence of EHBs will be investigated. Conclusions will be drawn in section 6.

2 DESCRIPTION OF THE PARAMETRIC MODEL

In the following, given the length-, velocity- and density-scale parameters, \tilde{r} , σ and $\tilde{\rho}$, respectively, it is convenient dealing with adimensionalized quantities, namely:

$$\begin{aligned} \text{radius } x &\equiv r/\tilde{r}; \\ \text{velocity } w &\equiv v/\sigma; \\ \text{mean total potential } W(x) &\equiv -\Psi(x)/\sigma^2; \\ \text{energy (per unit mass)} E &\equiv w^2/2 - W; \\ \text{density } \nu(x) &\equiv \rho(x)/\tilde{\rho}; \\ \text{cluster mass in stars, below the radius } x, \mathcal{M}(x) &\equiv M(x)/\tilde{\rho}\tilde{r}^3. \\ \text{BH mass } \mu &\equiv M_\bullet/\tilde{\rho}\tilde{r}^3. \end{aligned}$$

A suitable DF can be given by generalizing the King (1966) lowered Maxwellian, so as to include the BW76 DF below a proper ‘transition’ energy, i.e.

$$f(E) = \begin{cases} c(-E)^{1/4}, & \text{if } E < -W_{\text{BH}}, \\ (2\pi)^{-3/2}(e^{-E} - 1), & \text{if } -W_{\text{BH}} \leq E < 0, \\ 0, & \text{if } E \geq 0, \end{cases} \quad (1)$$

where the coefficient $c \equiv (2\pi)^{-3/2}(e^{W_{\text{BH}}} - 1)W_{\text{BH}}^{-1/4}$ assures the f continuity and W is defined so to have $W(x_t) = 0$ where x_t is the model ‘limiting radius’. The ‘transition’ potential $W_{\text{BH}} \equiv W(x_{\text{BH}})$ is considered to be the potential on the surface of the sphere, with radius x_{BH} , coinciding with the BHIR.

The BHIR can be defined as the *largest* sphere, centered at the BH position, in which the motion of the stars is dominated by the field generated by the compact object. This definition is coherent with the assumption of Maxwellian behaviour just outside this region (for $E \geq -W_{\text{BH}}$). Then, a reasonable condition for x_{BH} is that the enclosed mass in stars is a small fraction of the BH mass, i.e.

$$\mathcal{M}(x_{\text{BH}}) = 0.1\mu, \quad (2)$$

even if this forces to solve (as we will see later) an implicit equation that involves a mass profile that is only a-posteriori known. This condition is similar to that adopted in Merritt (2004); nevertheless we chose a smaller fraction (0.1 instead of 2) to ensure the validity of the power-law behaviour for $f(E)$ (see BW76, section IIIc).

The usually adopted formula $x_{\text{BH}} \sim GM_\bullet/\langle v^2 \rangle \tilde{r}$ (BW76; Baumgardt et al. 2004a,b) is not a-priori compatible with this BHIR definition. We verified that it gives rise to radii that are strongly underestimated with respect to our definition, because they yield typically $\mathcal{M}(x_{\text{BH}})/\mu \lesssim 10^{-4}$. Indeed, even if the BHIR has to be sufficiently small for the BH gravitational field to dominate the dynamics inside, on the other hand it must be large enough to make plausible the hypothesis of isothermal distribution outside it. This latter would not be realistic in an environment in which the BH still exerts a strong influence on the dynamics (BW76).

The DF of equation (1) guarantees the ‘dynamical equilibrium’ of the system, in the sense that, according to the Jeans theorem, it is a solution of the collisionless Boltzmann equation. The presence of a massive BH, assumed to be located *at rest* in the cluster centre, makes that the potential time-independence is preserved and thus the DF of equation (1) is still a valid equilibrium solution, because E remains an integral of motion. Therefore, one can proceed in the same manner as in obtaining usual King models, that is – as required by the self-consistency – just by solving, for $W(x)$, the adimensionalized Poisson’s equation in spherical symmetry

$$\frac{d^2W}{dx^2} + \frac{2}{x} \frac{dW}{dx} = -(4\pi G \tilde{\rho} \tilde{r}^2 \sigma^{-2}) \nu(W), \text{ for } x > 0, \quad (3)$$

where the origin is excluded to avoid the BH singularity and the stellar density, expressed as a function of W , is

$$\nu(W) = 4\pi \int_0^{\sqrt{2W}} f(E) w^2 dw = \begin{cases} \nu_1, & \text{if } W \leq W_{\text{BH}}, \\ \nu_2, & \text{if } W > W_{\text{BH}}, \end{cases} \quad (4)$$

where

$$\nu_1(W) \equiv e^W \text{erf}(\sqrt{W}) - \frac{2}{\sqrt{\pi}} \left(W^{1/2} + \frac{2}{3} W^{3/2} \right) \quad (5)$$

and

$$\nu_2(W) \equiv 4\pi c \int_{\sqrt{2W_{\text{BH}}}}^{\sqrt{2W}} \left(W - \frac{w^2}{2} \right)^{1/4} w^2 dw + \nu_1(W_{\text{BH}}) = 2^{7/2} \pi c g(W) W^{7/4} + \nu_1(W_{\text{BH}}). \quad (6)$$

The first term of equation (6) is the density corresponding to a polytropic stellar model with index = 7/4 (Binney & Tremaine 1987), with

$$g(W) = \int_0^\theta (\sin^{3/2} y - \sin^{7/2} y) dy, \quad (7)$$

where $\theta \equiv \cos^{-1} \sqrt{W_{\text{BH}}/W}$, $0 \leq \theta \leq \pi/2$.

The integral in equation (7) yields

$$g(W) = -\frac{4}{21} \left[F\left(\frac{\pi}{4} - \frac{\theta}{2}\right) - F\left(\frac{\pi}{4}\right) \right] - \frac{1}{42} (5 \cos \theta + 3 \cos 3\theta) \sqrt{\sin \theta} - \frac{4}{21} \left[F\left(\frac{\pi}{4} - \frac{\theta}{2}\right) - F\left(\frac{\pi}{4}\right) + (3\omega - 1)(1 - \omega)^{1/4} \frac{\sqrt{\omega}}{2} \right], \quad (8)$$

where $\omega \equiv W_{\text{BH}}/W$ and $F(\phi) \equiv \int_0^\phi (1 - 2 \sin^2 y)^{-1/2} dy$ is an elliptic integral of the first kind that can be accurately evaluated by standard numerical iterative procedures (see, e.g., Press et al. 1988, sect. 6.11).

As in standard King models, it is convenient to impose the relation

$$\tilde{r}^2 = \frac{9\sigma^2}{4\pi G \tilde{\rho}}. \quad (9)$$

With this choice equation (3) becomes

$$\frac{d^2W}{dx^2} + \frac{2}{x} \frac{dW}{dx} = -9\nu(W), \text{ for } x > 0, \quad (10)$$

that has a family of solutions depending only on the boundary conditions (with $x_0 > 0$),

$$\begin{aligned} \frac{dW}{dx}(x_0) &= W'_0, \\ W(x_0) &= W_0. \end{aligned} \quad (11)$$

Choosing $x_0 = x_{\text{BH}}$, these conditions define a two-parameters ($W'_{\text{BH}}, W_{\text{BH}}$) set of models¹, with all the others being just scaling parameters.

By the definition of BHIR it can be assumed that

$$\frac{d\Psi}{dr}(x_{\text{BH}}) = \frac{GM_\bullet}{(x_{\text{BH}} \tilde{r})^2} = \frac{G\mu}{x_{\text{BH}}^2} \tilde{\rho} \tilde{r}, \quad (12)$$

that, using equation (9), leads to

$$W'_{\text{BH}} = -\frac{9\mu}{4\pi x_{\text{BH}}^2}. \quad (13)$$

Thus, the whole set of models can be conveniently described by the pair (μ, W_{BH}) , while the solution inside the BHIR can be found by integrating backward equation (3) from x_{BH} to a given minimum radius, which we generally set equal to $0.1x_{\text{BH}}$.

Finally, the right value of x_{BH} must be a solution of equation (2) with $\mathcal{M}(x)$ given self-consistently by the model that uses x_{BH} itself as a BHIR radius. This value is found iteratively, evaluating the “new” x_{BH} through equation (2) with $\mathcal{M}(x)$ generated employing the previous value of x_{BH} . The process starts with an initial guessed $x_{\text{BH}} = GM_\bullet/3\sigma^2 \tilde{r}$ and is halted when the difference between two subsequent values is within a given tolerance.

2.1 Inclusion of a mass spectrum

The continuum stellar mass spectrum of the real cluster can be represented by a set of n stellar components, each one having a star mass m_k , a total mass M_k and a velocity parameter σ_k . The DF of the more realistic multimass case, f_{mm} , can be given as a linear combination of the f of equation (1) (see, e.g., Da Costa & Freeman 1976; Gunn & Griffin 1979):

$$f_{\text{mm}}(E) = \sum_{k=1}^n \alpha_k f_k(E) = \sum_{k=1}^n \alpha_k f(\beta_k E), \quad (14)$$

where α_k serve to reproduce the given mass function and $\beta_k \equiv \sigma^2/\sigma_k^2$.

A more rigorous treatment would require f_k to explicitly depend on m_k through the exponent of E in the DF inside the BHIR, as a consequence of mass segregation. This dependence was quantified by Bahcall & Wolf (1977) and then confirmed (at least partially) by means of Fokker-Planck (Murphy et al. 1991), N -body (Baumgardt et al. 2004b) and Monte-Carlo (Freitag et al. 2006a) simulations. Nevertheless, the small gain in ‘theoretical coherence’ might be vanquished by the use of a discrete set of stellar masses instead of the real continuous mass spectrum. Furthermore, the model would be complicated by the need of separate numerical quadratures in equation (4) for each mass class. For these reasons, we simplified the model construction by considering the same energy exponent ($-1/4$) in $f(E < -W_{\text{BH}})$, regardless of the stellar mass. However,

¹ In standard King models $W'_0 \equiv 0$ at $x_0 = 0$

the energy equipartition, responsible of mass segregation, can be still reproduced at the border of the BHIR by a suitable choice of β_k (see below).

Thus, the multicomponent Poisson equation has the same form of equation (10) apart from ν that is replaced by the total density

$$\nu_{\text{tot}}(W) \equiv \sum_{k=1}^n \frac{\alpha_k}{\beta_k^{3/2}} \nu(\beta_k W), \quad (15)$$

where ν is given here by equation (4).

Once a component is arbitrarily chosen as the ‘reference’ one, say the first one, without loss of generality it can be put $\sigma = \sigma_1$, i.e. $W = W_1$ and $\beta_1 = 1$. Then, since the set of α_k are constrained by the given set of M_k , the solutions of the Poisson equation are determined just by the boundary conditions (11) at $x_0 = x_{\text{BH}}$. Indeed, the set of $\beta_{k>1}$ can be fixed by the requirement of energy equipartition in the central region. To do that, the procedure described in Miocchi (2006) is applied at the radius² x_{BH} . In practice, once given σ and W_{BH} , we have

$$\beta_k = W_{\text{BH}}^{-1} \kappa^{-1} \left[\frac{m_1}{m_k} \kappa(W_{\text{BH}}) \right], \quad (16)$$

with κ the function defined in equation (8) of Miocchi (2006), and $\sigma_k^2 = \sigma^2 / \beta_k$.

Thus, W_{BH} and μ determine a 2-parameters family of models [through equation (13)] also in the multimass case. Note, furthermore, that f_k does now depend on m_k , through β_k .

As regards x_{BH} , the same iterative procedure described in the single-component case is employed to find the value that solves equation (2). Finally, as a consistency test, the velocity dispersion profile generated by the model is compared with that deduced by the spherical isotropic Jeans’ equation (Binney & Tremaine 1987),

$$\langle w^2 \rangle_J(x) = \frac{27}{4\pi\nu_{\text{tot}}(x)} \int_x^{x_t} \nu_{\text{tot}}(y) [\mathcal{M}(y) + \mu] y^{-2} dy, \quad (17)$$

and the model output $[\mathcal{M}(x), \nu_{\text{tot}}(x)]$ is accepted only if the difference between them keeps within a given tolerance.

3 SURFACE BRIGHTNESS PROFILES WITH IMBH

To understand how the presence of an IMBH influences the shape of a typical projected profile, it is instructive to examine the results of a single-mass model first. In Figs 1 and 2, various projected surface density profiles (Σ) are plotted, fixing $W_{\text{BH}} = 9.5$, for some of the models written on Table 1. As a comparison, a standard King model is also plotted with $W_0 = 9.5$.

As expected, we can see that the BH gives rise to a cuspy behaviour extended from the centre up to a radius that can be called the ‘cusp’ radius, x_{cu} , above which the much flatter core region begins. This radius, which is larger and larger as μ increases (see Table 1), was found to be well approximated – at least in the range of BH

Table 1. Relevant parameters for single-mass models generated with $W_{\text{BH}} = 9.5$. Some of them are plotted in Figs 1 and 2. μ is the dimensionless BH mass, M_{\bullet}/M is the BH mass in units of total cluster mass, c is the concentration defined according to Equation (18), x_{BH} is the BHIR radius, x_{cu} is the cusp radius, x_c is the core radius and s is the logarithmic slope of the projected surface density around x_{cu} .

μ	M_{\bullet}/M	c	x_{BH}	x_{cu}	x_c	s
no BH	0	2.2	0	0	0.92	0
0.05	5.9×10^{-4}	2.2	0.10	0.18	1.0	7.4×10^{-2}
0.2	2.4×10^{-3}	2.1	0.15	0.30	1.2	0.18
0.5	6.0×10^{-3}	1.8	0.16	0.56	2.2	0.25
0.8	8.4×10^{-3}	1.4	0.16	1.1	4.6	0.19
1	8.9×10^{-3}	1.1	0.15	1.9	8.5	0.14
1.4	9.0×10^{-3}	0.87	0.14	6.0	28	9.8×10^{-2}
1.5	9.3×10^{-3}	0.80	0.14	8.8	42	8.8×10^{-2}
1.6	1.0×10^{-2}	0.78	0.14	14	66	7.7×10^{-2}
1.8	1.8×10^{-2}	0.77	0.14	84	330	0.12
2	9.2	< 0	0.14	> x_t	3.1	> 1

masses studied here ($M_{\bullet}/M \lesssim 2$ per cent) – by the radius containing half the BH mass in stars $[\mathcal{M}(x_{\text{cu}}) = \mu/2]$. Furthermore, it is convenient to define the ‘core’ radius x_c as equal to the radius at which the surface brightness drops to 1/2 the value at x_{cu} (it is assumed that $x_{\text{cu}} = 0$ in the case of a standard King model). Indeed, it is important to adopt a concentration parameter that is unambiguously defined even if a density cusp is present. In particular, the parameter

$$c \equiv \log \left(\frac{x_t}{x_c} \right) \quad (18)$$

is preferable to the standard King concentration parameter $c_K = \log(x_t)$, because this latter is based on the length-scale \tilde{r} that has no immediate relation with any relevant morphological parameter for our IMBH models³. However, it has been checked that an IMBH model with a given c , yields a profile that is matched quite well, in the core and in the tidal region, by that of a standard King model having $c_K = c$. Of course, by comparing our definition of x_{cu} with equation (2) it is clear that the cusp extends always beyond the BHIR.

The projected density profiles depicted in the Figures show also the goodness of the definition of x_c , because the core radius corresponds actually to the location of the ‘knee’ of the curves – where the flatter core region ends – in analogy to a standard King profile. From these profiles (plotted as a function of the radius measured in unit of x_c) three relevant features can be immediately noticed:

- (i) the projected density in the core region is not as flat as in standard King model, (see inset in Figs 1b and 2b)
- (ii) the presence of a central IMBH reduces significantly the concentration of the profile in comparison with a BH-free model with $W_0 = W_{\text{BH}}$, and
- (iii) the concentration *decreases* for increasing μ .

² Because only for $x > x_{\text{BH}}$ all f_k are lowered Maxwellians.

³ On the contrary, in King models $x_c \simeq 1$, i.e. the core radius is $\simeq \tilde{r}$.

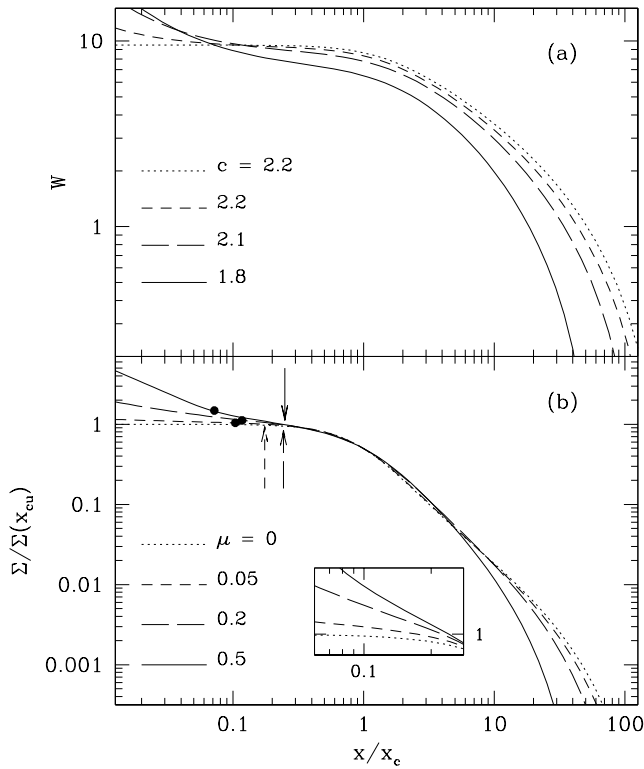


Figure 1. (a) Behaviour of the potential and (b) projected surface density profile (scaled so as to give $\Sigma = 1$ at the cusp radius) for single-mass models with $W_{\text{BH}} = 9.5$ and with various IMBH mass as indicated ($\mu = 0$ means a standard King model, with $W_0 = 9.5$). The dots mark the BHIR radii, while the arrows indicate the cusps radii (x_{cu}). The panel (b) inset shows the profiles in the core region around x_{cu} . The concentration parameters are also reported in panel (a).

These features are confirmed (as we will see later) in the case of multimass models, too.

The last two points can be easily understood from the behaviour of the potential (Figs 1a and 2a) that, at x_{BH} , has a different slope when compared with the (practically flat) King model. The potential with the BH decreases below W_{BH} , then becomes flatter in the core (before dropping in the tidal region) leading the system to a lower concentration profile in comparison with the BH-free case. This suggests that the presence of a IMBH induces profiles with a large core.

Note, from Table 1, the rapid growth of the cusp radius for $\mu > 1$; for $\mu = 2$, it becomes even larger than the limiting radius making, in fact, $\Sigma(x)$ to “jump” to a completely cuspy behaviour (not shown in the Figures), without any recognizable core. Since this leads to $M_\bullet > M$, such kind of configurations are discarded throughout our analysis, as unrealistic for globular clusters. Thus, reasonable values of the BH mass at the centre of GCs are compatible *only* with a core-like profile. The density cusp is confined in the very inner region of the core.

All this is in remarkable agreement with the results of Baumgardt et al. (2005) and Trenti et al. (2007), obtained by means of collisional N -body simulations including IMBH. These simulations have shown that the presence of an IMBH initially enhances the rate of ex-

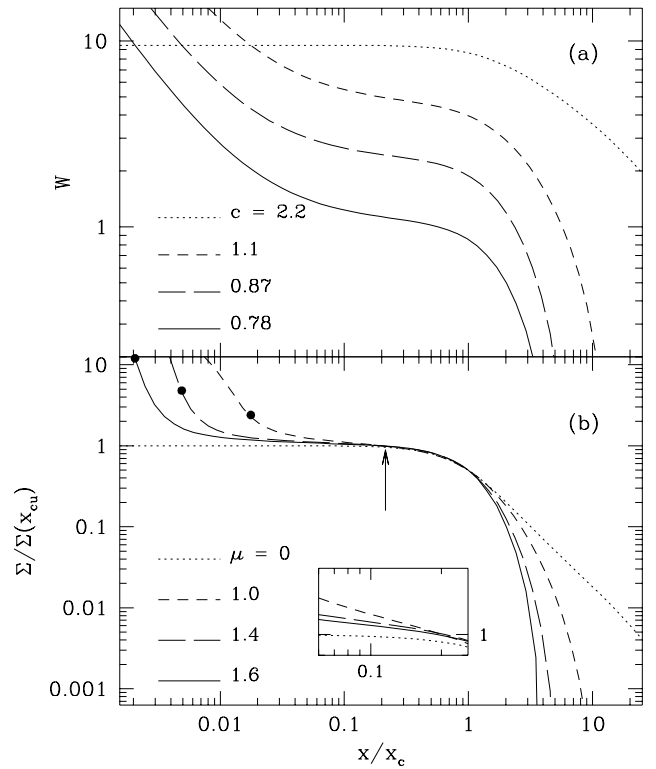


Figure 2. The same as in Fig. 1 for models with higher BH mass. Since in this case the cusp radii are nearly equal, only one arrow is plotted.

change of energy in close encounters among stars moving in the cusp region; this gives rise to a strong cluster expansion which, in turn, yields final profiles well fitted by King models, with a relatively low concentration (see also Baumgardt et al. 2004a,b).

Finally, the apparent contradiction that can be seen in Figs 1–2 of a decreasing BHIR radius for increasing BH masses, is actually due to the scaling of the radius with x_c and to the fact that the core radius grows quite rapidly while x_{BH} is nearly constant (see Table 1). The decrease of the ratio x_{BH}/x_c is a consequence of the lower and lower concentration that these models show for growing BH masses. Another consequence is the unexpected decrease of the logarithmic slope (s , with $\Sigma \sim x^{-s}$) of the surface density around x_{cu} , that can be seen for $\mu > 0.5$ (see Table 1 and Fig. 2b inset).

3.1 The multimass case

At this point, one could study in more detail the dependence on the BH mass of both c and the slope of $\Sigma(x)$ in the core region. Nevertheless, it is more appropriate to make this analysis directly in the multimass context, which is (for globular clusters) a much more realistic scenario than that of the single-mass case, because the mass-segregation could heavily change the effect of the presence of the BH in the brightness profile (Baumgardt et al. 2005).

Thus, a stellar mass spectrum is included assuming a Salpeter mass function ($dN \propto m^{-1.35} d \log m$) and

Table 2. Values for the components used in the multimass model. MS = main sequence stars; G = giants; HB = horizontal branch stars; WD = white dwarfs (from Côté et al. 1995).

k	mass range (M_{\odot})	M_k/M	$m_k (M_{\odot})$	$(L/M)_k$	σ_k/σ	content
1	0.75–0.83	4.9×10^{-2}	0.79	10	1	MS, G, HB
2	4–8 ^a	3.9×10^{-2}	1.2	0	0.81	WD
3	0.65–0.75 ^b	0.18	0.70	0.19	1.1	MS + WD
4	0.55–0.65	9.3×10^{-2}	0.60	6.5×10^{-2}	1.2	MS
5	0.45–0.55 ^c	0.24	0.50	2.3×10^{-2}	1.3	MS + WD
6	0.35–0.45	0.16	0.39	1.0×10^{-2}	1.6	MS
7	0.25–0.35	0.24	0.29	4.9×10^{-3}	5.7	MS

^a Progenitors mass range that yield $1.2 M_{\odot}$ WD.

^b Including a $0.7 M_{\odot}$ WD population from progenitors with mass $1.5\text{--}4 M_{\odot}$.

^c Including a $0.5 M_{\odot}$ WD population from $0.83\text{--}1.5 M_{\odot}$ progenitors.

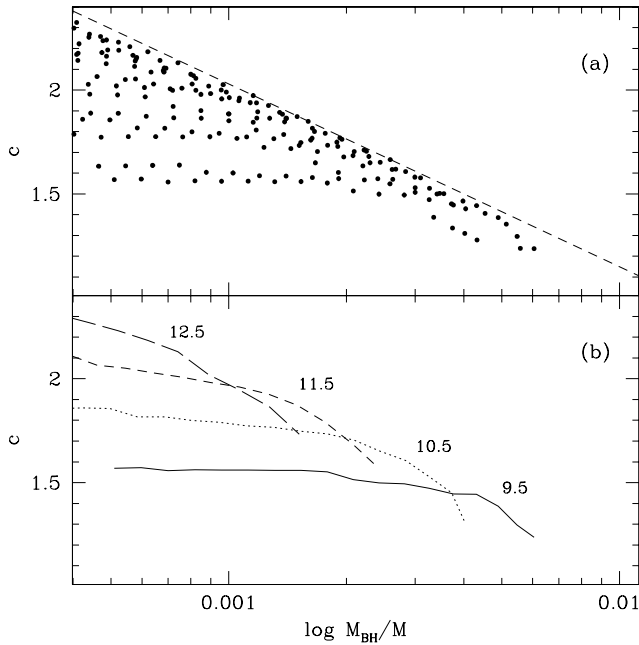


Figure 3. (a) Concentration parameter obtained for a grid of values of M_{\bullet}/M , and W_{BH} ; no realistic models can be generated above the dashed line. (b) Behaviour of c as a function of BH mass for some values of W_{BH} , as indicated.

considering 7 mass bins in the range $0.25 - 0.83 M_{\odot}$, along with light and heavy remnants, following the prescriptions of Côté et al. (1995). Nevertheless, their lightest mass class was not included because it is below the lower mass limit predicted, under energy equipartition, in Miocchi (2006). See Table 2 for the list of parameters for the adopted stellar components.

The qualitative behaviours of the apparent concentration and of the Σ slope as a function of the BH mass discussed in the single-component case, are basically confirmed by the curves plotted in Figs 3b–4b. They refer to a grid of models computed in the range $15 \leq W_{\text{BH}} \leq 9.5$ and $10^{-2} \leq \mu \leq 0.15$. In this case the concentration has been evaluated on the total projected surface brightness

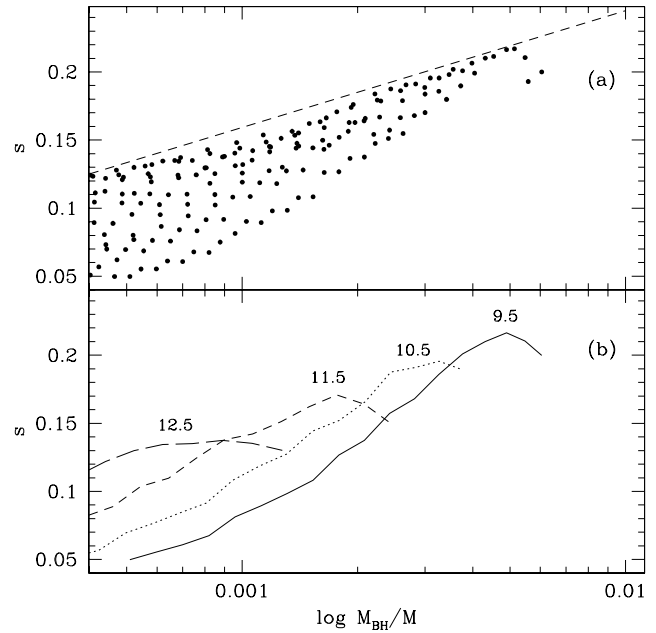


Figure 4. As in Fig. 3 for the logarithmic slope of the surface brightness at the cusp radius.

profile, $I(x)$, and the logarithmic slope s is again such that $I \sim x^{-s}$. It is worth noting that:

- (i) c decreases monotonically with the BH mass
- (ii) according to our model, IMBHs with $M_{\bullet} \gtrsim 10^{-3} M$ can exist only for non-collapsed distributions ($c \lesssim 2$) exhibiting a logarithmic slope in the core which is $\lesssim 0.25$ for reasonably low BH masses ($M_{\bullet} \lesssim 10^{-2} M$)
- (iii) s increases for growing BH mass up to a certain value, above which the lower concentration achieved makes the core region to be much wider than the cusp region causing the decrease of s .

These features fully confirm the Baumgardt et al. (2005) findings.

In Fig. 3b it is apparent a certain degree of self-similarity of the various curves; of course, lower concentrations can be in principle obtained starting from lower

W_{BH} – though this imposes an even higher mass cut-off of the stellar mass function at the low-mass end in order to ensure energy equipartition. Thus, no lower limit on c can be fixed. On the contrary, an upper limit to the concentration exists (roughly indicated by the dashed line in Fig. 3a). The same argument holds for s (Fig. 4), for which lower values could be obtained for lower W_{BH} . Thus, combining the upper limits of the two quantities, a range of admitted values is found for the BH mass:

$$11.6s - 4.85 \lesssim \log \left(\frac{M_{\bullet}}{M} \right) \lesssim -1.14c - 0.694. \quad (19)$$

3.1.1 The effect of mass segregation

The presence of mass segregation (as due to the imposed energy equipartition at x_{BH}) is evident in Fig. 5. Three component are represented: the brightest component, the heavy remnants one and the lightest MS stars component ($k = 1, 2$ and 7 , respectively, in Table 2). The first component is the one that gives almost all the cluster luminosity. The model has been generated with $W_{\text{BH}} = 9.5$ and $\mu = 0.155$, corresponding to $M_{\bullet}/M = 6 \times 10^{-3}$.

In the core region the lightest (heaviest) stars have the highest (lowest) velocity dispersion and, consequently, the least (most) concentrated density profile. The lightest star component is practically unaffected by the presence of the BH, while inside the BHIR the density cusp is particularly evident for the most massive stars.

We note that the density of each component must have the same asymptotic BW76 behaviour $\sim x^{-\gamma}$, with $\gamma = 7/4$ (i.e. $\sim W^{7/4}$), because it was assumed for simplicity that all the f_k in equation (14) have the same functional form. Nevertheless, how much deep one has to go towards the centre to find the $x^{-7/4}$ cusp depends on β_k and, in turn, on the component stellar mass. This is because the density of the k th component is a function of $\beta_k W \propto \sigma_k^{-2}$ [equation (15)]; thus, the higher the velocity dispersion of the stars are, the more inward the region where the ‘isothermal plateau’ prevails extends, the flatter the density is at a fixed radius.

In this respect, in Fig. 6 the log slope γ of the space mass density in the cusp region is plotted as a function of the stellar mass. The slope is evaluated well inside the BHIR, namely at $\sim x_{\text{BH}}/5$, i.e. where the enclosed mass in stars is of order $10^{-2} M_{\bullet}$. It can be noticed that sufficiently massive stars ($m \gtrsim 0.6 M_{\odot}$) show a slope close to the linear relation $\gamma \simeq 1.8m/(0.8 M_{\odot})$, of the kind of that predicted by the multicomponent Fokker-Planck solutions of Bahcall & Wolf (1977) and then confirmed by Murphy et al. (1991). Since low mass stars have a very inner cusp region, they exhibit $\gamma < 1.5$, in accordance to what found in Baumgardt et al. (2004a). The authors also found a particularly low slope for intermediate mass stars (see figure 6), probably because in their simulations particles did not reach the $x^{-7/4}$ regime (see the discussion in Freitag et al. 2006a, and figure 5). On the other side, Hopman & Alexander (2006) including energy equipartition in the numerical integration of multicomponent Fokker-Planck equations, reported power-law density behaviour with a high slope ($\simeq 2$) for massive objects (stellar BHs around the Galactic supermassive BH).

However, for the mass range and mass function considered here, we found that the $\gamma - m$ relation is well fitted by the law $\gamma = [m/(1 M_{\odot}) - 0.29]^{0.33} + 1$. Although we cannot draw really general conclusions, it can be stated that our prescription to enforce energy equipartition generates results compatible with the findings of the various studies related to mass segregation phenomena around a massive BH (see also Alexander 1999; Merritt 2004; Hopman & Alexander 2006).

To give an indication on the chance of detecting the IMBH by means of observation of velocity dispersion profiles⁴, let us suppose that this model represents a luminous and nearby cluster (with $c \simeq 1.2$), located at a distance of 5 Kpc, with a central surface brightness $I_0 \sim 2 \times 10^4 L_{\odot} \text{ pc}^{-2}$. If its core radius is a typical $r_c \sim 2$ pc, the BHIR radius is $r_{\text{BH}} = 0.094$ pc. Moreover, let us assume that all the luminosity is given by the brightest component (that with $k = 1$ in Table 2), whose stars would have, at that distance, $V \simeq 16$. The number of these stars below the BHIR radius can be estimated by

$$N_1 \simeq I_0 \pi r_{\text{BH}}^2 \left[\left(\frac{L}{M} \right)_1 m_1 \right]^{-1}, \quad (20)$$

which gives $N_1 \simeq 70$, thus it would be rather difficult to obtain a statistically significant set of velocity dispersion measures so as to resolve the velocity cusp.

This is confirmed by the example reported in Fig. 5a, in which such measures were done for a set of annuli around the cluster centre. The error bars are evaluated by the usual formulas (see, e.g., Jones 1970; McNamara et al. 2003), assuming an rms error on the single star velocity determination of $\simeq 0.7 \text{ km s}^{-1}$ (similar to, e.g., the typical accuracy level in the FLAMES-GIRAFFE Very Large Telescope observations by Milone et al. 2006, for stars with the same V) and treating the model σ_p profile as if it were the observed velocity dispersion profile, with a typical $\sigma = 10 \text{ km s}^{-1}$. Despite of the relatively high I_0 and low cluster distance, it is hard to identify a cusp in velocity for such a non-collapsed cluster. Even if in a real observation the error bars could be smaller because of a larger number of stars actually observable, the detection of a velocity cusp is certainly much more difficult than for high-concentration clusters (see, e.g., Gerssen et al. 2002; Gerssen 2004; Gebhardt et al. 2005).

In general, for the grid of multimass models generated, we found that $x_{\text{BH}}/x_c \sim 0.07 \pm 0.05$, a ratio that will be used in the following section, to give an estimate about N_1 for the candidates clusters.

Finally, note that the radius – measured in units of x_c – at which the velocity dispersion is mostly affected by presence of the BH (where it follows a keplerian behaviour) is ~ 0.02 for the luminous component (Fig. 5a). This factor is equal to about $3M_{\bullet}/M$, in good agreement with the relation found by Baumgardt et al. (2005).

⁴ Because of the assumed isotropy, line-of-sight velocity and proper motion dispersion are equivalent.

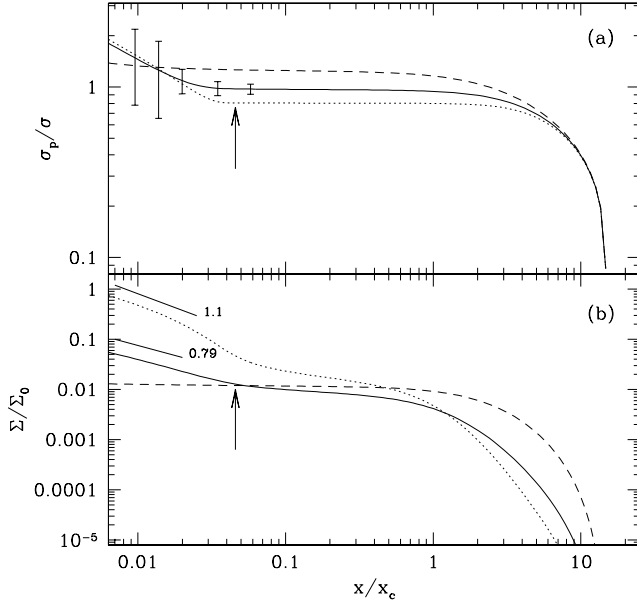


Figure 5. (a) Line-of-sight velocity dispersion profile and (b) projected surface density (normalized to the central value of the heavy remnants component) for the multimass model described in the text. Three components are shown: giant and turnoff stars (solid line), heavy dark remnants (dotted), lightest main sequence stars (dashed). The central logarithmic slope of Σ are also reported for giants and heavy remnants. The vertical arrows indicate the BHIR radius. The error bars refer to simulated velocity dispersion measures (see text).

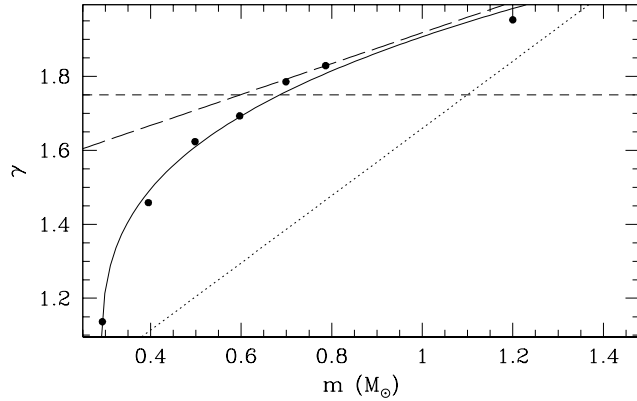


Figure 6. Logarithmic slope of the space density of stars evaluated for the various components (dots) inside the cusp region (at $x = 0.01x_c$) and fitted by the law $(m - 0.29)^{0.33} + 1$ (solid line). The short-dashed line is the $7/4$ predicted value in the single-mass context. The fit from the Baumgardt et al. (2004b) results (dotted line) and the Bahcall & Wolf (1977) relation (long-dashed) are also reported.

4 BLACK HOLE MASS ESTIMATED FROM CLUSTER PROFILE

Exploiting equation (19), we can now make a tentative estimate of the IMBH mass range in clusters, from their concentration and from the slope of the central surface brightness profile. To this purposes, the recent and detailed analysis of WFPC2/*HST* observations made by

NG06 for 38 galactic globular clusters, provide the necessary set of data. Moreover, we also considered the controversial case of the cluster G1 in M31, for which s is estimated by using the recent ACS/*HST* photometric profile published in Gebhardt et al. (2005) and the total mass and concentration taken by Meylan et al. (2001).

From the whole list, 15 clusters were excluded (marked with ‘x’ in the last column of Table 3) because they yield, from equation (19), a lower limit for the BH mass higher than the upper one. All of core-collapsed clusters are in this subset (including G1), together with those having a steep central brightness profile ($s \gtrsim 0.2$) despite of being not very concentrated, like, e.g., NGC 6535 (that has $c = 1.3$ and $s \simeq 0.5$). Of course, the presence of a IMBH cannot be completely ruled out for these clusters. It can only be stated that such a presence is incompatible with the stars phase-space distribution of the form given by equations (1) and (14). Moreover, there are 18 clusters (marked with ‘o’) having very low (or negative) central slope, for which the lower limit in equation (19) is $< 100 M_\odot$; conservatively, they were considered as clusters without IMBH. This because the model is based on the assumption that M_\bullet is much greater than any single stellar mass, so as to be considered at rest in good approximation. Thus, as regards these clusters, the model cannot provide sufficiently stringent and reliable predictions; accurate individual parametric fits would be necessary to this aim. Note, however, that the NG06 uncertainties on the measures of s are rather large. This error is not taken into account in the present analysis.

The relevant parameters of the remaining 6 candidates clusters are written in Table 4. Their predicted IMBH mass range is plotted both vs. the total cluster V-band luminosity and the observed velocity dispersion (Fig. 7). It is apparent that M_\bullet/M has only a weak dependence on L while the BH mass tends to increase with σ_{obs} . To quantify these trends, weighted least-squares fits were computed (following the prescriptions of Press et al. 1988, sect. 15.2) neglecting, for simplicity, the uncertainties both in L and in σ_{obs} . The resulting fits are

$$\log \left(\frac{M_\bullet}{M} \right) = (-1.8 \pm 1.9) + (-0.22 \pm 0.36) \log \left(\frac{L}{L_\odot} \right) \quad (21)$$

with $\chi^2_{\text{fit}} = 0.34$ at a confidence level $P(\chi^2 > \chi^2_{\text{fit}}) = 0.99$, and

$$\log \left(\frac{M_\bullet}{M_\odot} \right) = (2.0 \pm 1.7) + (0.9 \pm 1.5) \log \left(\frac{\sigma_{\text{obs}}}{\text{km s}^{-1}} \right) \quad (22)$$

with $\chi^2_{\text{fit}} = 0.79$ and $P(\chi^2 > \chi^2_{\text{fit}}) = 0.94$. The cluster luminosity was chosen as an independent variable because its measure is much more reliable and directly linked to observations than the dynamically estimated total masses (Pryor & Meylan 1993).

However, assuming a uniform global mass-to-light ratio equal to that averaged among the candidates clusters, $\simeq 3.1(M/L)_\odot$, equation (21) gives $M_\bullet \sim 0.02(M/M_\odot)^{0.78 \pm 0.36} M_\odot$, which is in good agreement with the $M_\bullet \propto M$ relation between super-massive BHs in galactic nuclei and the bulge mass (Magorrian et al. 1998), and between the mass of the compact nuclei and

that of the host spheroid in nucleated dwarf galaxies (Côté et al. 2006; Wehner & Harris 2006).

Notice that a certain (though weak) positive correlation $c - L$ exists for clusters in our Galaxy (Djorgovski & Meylan 1994); this correlation is also recognised in the NG06 set of clusters: excluding those with the arbitrary value $c = 2.5$, we found $c \sim 0.4 \log M$. Thus, because of the negative factor multiplying c in the right-hand side of equation (19), one can say that this link actually tends to ‘cancel’ the link $M_\bullet - M$ (it would give $M_\bullet \lesssim M^{0.5}$). Hence, relation (21) seems not to be merely related to the observed correlation between globular clusters concentration and luminosity.

As regards relation (22), it turns out to be very different from the law $M_\bullet \sim \sigma_{\text{obs}}^{4.8}$ found by Ferrarese & Merritt (2000) for galactic bulges (see also Tremaine et al. 2002). The reason of this discrepancy can be understood by the same argument the authors presented for explaining the relation they found: the $M_\bullet - \sigma_{\text{obs}}$ link is a consequence of the fundamental relation $M_\bullet \propto M$. In galaxies, this relation and the $M \sim L^{5/4}$ and $L \sim \sigma_{\text{obs}}^4$ laws lead indeed to $M_\bullet \sim \sigma_{\text{obs}}^5$. In globular clusters, on the other hand, the observed trends $M \sim L$ and $L \sim \sigma_{\text{obs}}^{5/3}$ (Meylan & Héggie 1997) yield, through equation (21), $M_\bullet \sim \sigma_{\text{obs}}^{1.3}$, which is compatible with the relation (22).

However, since in old globular clusters the secular collisional relaxation has certainly had a substantial influence on the dynamics within the core region, it is reasonable to expect only a weak correlation between M_\bullet and the presently observed core velocity dispersion. Moreover, as discussed in sect. 3.1.1, it is rather improbable that σ_{obs} could provide a really reliable and accurate indication on the velocity dispersion in the inner cusp region; in fact, N_1 is rather low (< 60) for the candidates clusters (see Table 4). Conversely, the cluster total mass, despite of the tidal erosion, should keep a tighter link with the environmental conditions at the first stage of the cluster life (at least for massive clusters), when IMBHs formation are thought to have occurred (e.g. Gürkan et al. 2004).

To improve our capability of identifying the presence of IMBHs, it is important to search for other indicators that could be related to the gravitational influence of the compact object on the surrounding cluster stars. In this context, the presence of an extreme horizontal branch in the colour-magnitude diagram (CMD) may be a valid indicator, as we will see in the next Section.

Not surprisingly, however, another indication in favour of the presence of IMBHs at the centre of our candidates clusters, is that their r_c/r_h ratio – as directly evaluated from the values listed in the Harris catalogue, see Table 4 – is significantly higher than the maximum value (~ 0.05) suggested by Trenti (2006) for clusters that do not harbour IMBHs, because they are not affected by the enhanced core expansion occurring when such an object reside inside a relaxed cluster.

To conclude this section, it is worth noting the similarity of the surface brightness profiles observed by NG06 (plotted in their Fig. 7) with those illustrated here in Figs. 1b and 5b. By inspecting those corresponding to our candidates clusters, the similarity is rather evident for M80 and M13. Indeed, these clusters show a clear

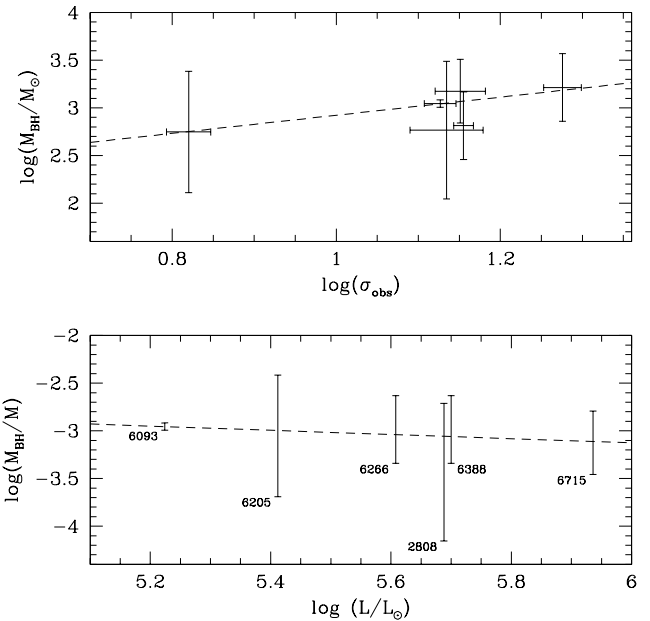


Figure 7. Upper panel: BH mass of the candidates clusters plotted vs. the observed central velocity dispersion (in km s^{-1}); lower panel: log of the ratio M_\bullet/M plotted against total cluster luminosity. The dashed lines are the weighted least-squares fits $\log(M_\bullet/M) = -1.8 - 0.22 \log(L/L_\odot)$ and $\log(M_\bullet/M_\odot) = 2 + 0.9 \log(\sigma_{\text{obs}})$.

transition between a core and a cusp region. Note that they are the only ones, in the NG06 set, in which this feature is clearly observed. Thus, more detailed individual studies, also through parametric fits of the profiles based on the model discussed here, certainly deserve to be carried out for them. Note, finally, that our candidates list has 4 clusters in common with the set of 9 clusters that Baumgardt et al. (2005) suggest as possibly harbouring IMBHs.

5 THE IMBH – EHB CONNECTION

Let us assume that the loss of envelope mass is the dominant effect suffered by a giant during a close passage around the IMBH (‘tidal stripping’), and that it becomes an EHB star because of its uncovered underlying hotter layers (Rich et al. 1997; Alexander 2005). Given that $r_{\text{tid}} = R_*(M_\bullet/m)^{1/3}$ is the distance from the IMBH below which the tidal interaction with a star (with radius R_* and mass m) can significantly perturb its internal structure (see, e.g., Freitag & Benz 2002; Baumgardt et al. 2006), then the order of magnitude of the rate of tidal stripping events, S , can be estimated as

$$S \simeq n_0 \sigma_0 \pi r_{\text{tid}}^2 \left(1 + \frac{2GM_\bullet}{r_{\text{tid}} \sigma_0^2} \right)^2, \quad (23)$$

where n_0 and σ_0 are, respectively, the typical stellar number density and velocity dispersion in the cusp region, and where the gravitational focusing is taking into account in the estimate of the cross-section of the single stripping event (Freitag et al. 2006b).

Table 3. Globular clusters in the NG06 set. L is the total luminosity in the V -band evaluated from M_V listed in the Harris catalogue. c = cluster concentration (from the Harris catalogue; ‘:’ denotes a core-collapsed cluster). s is the logarithmic slope (from NG06, with opposite sign). $M_{\bullet,1}/M$ and $M_{\bullet,2}/M$ are the lower and upper limits of M_{\bullet}/M as from equation (19). M is the total cluster mass taken, if available, from the parametric estimates in Pryor & Meylan (1993), while those marked with a ‘:’ are estimated by assuming a uniform global mass-to-light ratio = 2. EHB₁ marked clusters are those with a Harris (1996) HB type = 0. EHB₂ clusters are those having $\log(T_{\text{effHB}}) > 4.3$ in the Recio-Blanco et al. (2006) list. Last column: ‘•’ denotes a candidate cluster; ‘×’ a cluster having $M_{\bullet,1} > M_{\bullet,2}$ and ‘o’ a cluster with $M_{\bullet,1} < 100 M_{\odot}$. Not available data are indicated by

NGC number	$\log(L/L_{\odot})_V$	c	s	$\log(M_{\bullet,1}/M)$	$\log(M_{\bullet,2}/M)$	$\log(M/M_{\odot})$	EHB ₁	EHB ₂	case
104 (47 Tuc)	5.7	2.03	0	−4.85	−3.01	6.1			o
1851	5.26	2.32	0.38	−0.442	−3.34	6.0			×
1904 (M79)	5.12	1.72	0.03	−4.50	−2.65	5.2	✓	✓	o
2298	4.45	1.28	0	−4.85	−2.15	4.8:		...	o
2808	5.69	1.77	0.06	−4.15	−2.71	6.2	✓	✓	•
5272 (M3)	5.5	1.84	0.05	−4.27	−2.79	5.8		...	o
5286	5.38	1.46	0.28	−1.60	−2.36	5.5		...	×
5694	5.06	1.84	0.19	−2.65	−2.79	5.4			×
5824	5.47	2.45	0.36	−0.67	−3.49	6.6		✓	×
5897	4.82	0.79	0.04	−4.39	−1.59	5.1:		...	o
5904 (M5)	5.46	1.83	−0.05	−5.43	−2.78	5.6			o
6093 (M80)	5.22	1.95	0.16	−2.99	−2.92	6.0	✓	✓	•
6205 (M13)	5.41	1.51	0.1	−3.69	−2.41	5.8	✓	✓	•
6254 (M10)	4.92	1.4	−0.05	−5.43	−2.29	5.4	✓	...	o
6266 (M62)	5.61	1.7	0.13	−3.34	−2.63	5.8		✓	•
6284	5.12	2.5:	0.55	1.53	−3.54	5.4			×
6287	4.88	1.6	0	−4.85	−2.52	5.2:			o
6293	5.04	2.5:	0.67	2.92	−3.54	5.6		...	×
6341 (M92)	5.21	1.81	0.01	−4.73	−2.76	5.3		...	o
6333 (M9)	5.11	1.15	0	−4.85	−2.00	5.4:		...	o
6352	4.52	1.1	−0.02	−5.08	−1.95	4.8:		...	o
6388	5.7	1.7	0.13	−3.34	−2.63	6.2			•
6397	4.58	2.5:	0.37	−0.56	−3.54	5.4			×
6441	5.79	1.85	0.02	−4.62	−2.80	6.2			o
6535	3.83	1.3	0.5	0.95	−2.18	4.2		...	×
6528	4.56	2.29	0.1	−3.69	−3.30	4.9:		...	o
6541	5.28	2:	0.41	−0.094	−2.97	5.6		...	×
6624	4.93	2.5:	0.32	−1.14	−3.54	5.2			×
6626 (M28)	5.20	1.67	−0.03	−5.20	−2.60	5.4		...	o
6637 (M69)	4.99	1.39	−0.09	−5.89	−2.28	5.3:			o
6652	4.60	1.8	0.57	1.76	−2.75	4.9:			×
6681	4.78	2.5:	0.82	4.66	−3.54	5.2		✓	×
6712	4.93	0.9	−0.02	−5.08	−1.72	5.0		...	o
6715 (M54)	5.94	1.84	0.12	−3.46	−2.79	6.3		...	•
6752	5.02	2.5:	0.03	−4.50	−3.54	5.2	✓	...	o
7078 (M15)	5.6	2.5:	0.66	2.81	−3.54	6.3	✓	✓	×
7089 (M2)	5.54	1.8	−0.05	−5.43	−2.75	6.0		✓	o
7099 (M30)	4.90	2.5:	0.57	1.76	−3.54	5.3			×
G1 ^a	6.31	2.5	0.16	−2.99	−3.54	7.0	×

^a L and s comes from Gebhardt et al. (2005); c and M are taken from Meylan et al. (2001).

For giants having $R_* \sim 100 R_{\odot}$ and $m = m_1$, one has $r_{\text{tid}} \simeq 2.5 \times 10^{-5}$ pc and taking, from the example discussed in section 3.1.1, $n_0 \simeq 3N_1/4\pi r_{\text{BH}}^3 \simeq 2 \times 10^4 \text{ pc}^{-3}$, $\sigma_0 \simeq 20 \text{ km s}^{-1}$ and $M_{\bullet} = 10^3 M_{\odot}$, one has $S \simeq 7 \times 10^{-7} \text{ yr}^{-1}$, which means that of order of 100 stripping events can occur within a HB stars lifetime ($\sim 10^8 \text{ yr}$), generating a significant population of EHB stars. Incidentally, this population could have an integrated luminosity ($10^2 - 10^4 L_{\odot}$, mainly in the UV band), compatible with the far-UV excess showed by some – even metal-rich – clusters (e.g. NGC 6388, see Rich, Minniti & Liebert 1993),

while, on the contrary, it would be clearly insufficient if one considered stripping events due to close encounters between *stars* only, as already pointed out by Rich et al. (1997). Thus, it is reasonable to expect that the existence of an EHB is favoured by the presence of an IMBH. To test this hypothesis, we rely on the classification made in the Harris catalogue (revised on February 2003). The author re-analysed various set of CMD observations (mainly those by Piotto et al. 2002), in the intent of updating the Dickens (1972) HB type, introducing a new type (= 0) just to account for clusters having a prominent EHB.

Table 4. Candidates clusters set. I_0 is the central surface brightness estimated from μ_V in Harris (1996) using equation (5) in Djorgovski (1993). r_c is the core radius in pc, estimated from the angular value and the cluster distance listed in the Harris catalogue. $M_{\bullet,1}$ and $M_{\bullet,2}$ are in M_\odot and calculated using M from Table 3. σ_{obs} is the central observed velocity dispersion taken from Pryor & Meylan (1993) or, marked with ‘:’, from Dubath, Meylan & Mayor (1997). M/L is the mass-to-light ratio in solar unit. r_c/r_h is the ratio between the core and the half-mass radius, directly estimated from Harris (1996). N_1 is the estimate of the no. of giants below x_{BH} from equation (20) assuming $r_{\text{BH}} = 0.07r_c$. The other symbols have the same meaning as in Table 3.

NGC number	$\log(L/L_\odot)$	I_0 ($L_\odot \text{ pc}^{-2}$)	r_c	$M_{\bullet,1}$	$M_{\bullet,2}$	M/L	EHB ₁	EHB ₂	σ_{obs} (km s ⁻¹)	r_c/r_h	N_1
2808	5.69	3×10^4	0.73	110	3.1×10^3	3.2	✓	✓	13.7 ± 1.4 :	0.34	31
6093 (M80)	5.22	2.94×10^4	0.44	10^3	1.2×10^3	6	✓	✓	13.4 ± 0.6	0.23	11
6205 (M13)	5.41	6.68×10^3	1.7	130	2.4×10^3	2.4	✓	✓	6.62 ± 0.41 :	0.52	40
6266 (M62)	5.61	2.54×10^4	0.36	290	1.5×10^3	1.5		✓	14.3 ± 0.4	0.15	6
6388	5.7	5.31×10^4	0.35	720	3.7×10^3	3.2			18.9 ± 0.8 :	0.18	13
6715 (M54)	5.94	4.14×10^4	0.86	700	3.2×10^3	2.3		...	14.2 ± 1.0 :	0.22	59

Thus, clusters with the HB type = 0 are considered as having EHB (they are marked in the EHB₁ column of Table 3). Then, we studied the probability distribution of finding a given number, N_{EHB} , of clusters with an EHB, in a set as large as our candidates clusters set. To this purpose, a large number of subsets made up of 6 clusters each, were extracted *at random* from the NG06 list. Then, N_{EHB} was evaluated for each subset and a frequency distribution was computed (see the solid histogram in Fig. 8). The result is that the probability to get *by chance* a set of 6 clusters with $N_{\text{EHB}} \geq 3$ (i.e. with N_{EHB} equal to or greater than that in our candidates clusters subset) is only $\simeq 0.063$. This, from a statistical point of view, means that the hypothesis of the *independence* between the presence of an IMBH and the presence of an extended HB blue tail can be rejected at a confidence level $\gtrsim 90$ percent.

However, the Harris new HB type was assigned to clusters with an high relative proportion of blue subdwarfs population in comparison with that at the redder side of the RR Lyrae region of the HB (Harris, private communication), whereas the determination of the presence of the EHB *regardless* of the other HB peculiarities would be more appropriate to our purposes. The various parameters defined by Fusi Pecci et al. (1993) to characterize the HB morphology are unsuitable as well, because they are mainly concerned with the length of the various portions of the HB in the CMD and their sample contains only very few clusters of the NG06 list. For these reasons, we chose considering the maximum effective temperature, T_{effHB} , evaluated by Recio-Blanco et al. (2006) (see their table 1) for the HB stars of a clusters set that includes a significant part of the NG06 sample.

In this case, an EHB was considered as present when $\log(T_{\text{effHB}}) > 4.3$ (i.e. $T_{\text{effHB}} \gtrsim 20,000$ °K, see e.g. Moehler 2001; Rosenberg, Recio-Blanco & García-Marín 2004). EHB clusters classified this way are signed in the ETB₂ column of Table 3. The visual inspection of the Piotto et al. (2002) CMDs – which the Recio-Blanco et al. (2006) evaluations are based on – confirms how in these clusters the EHB stars are clearly visible and reach downward a V magnitude as faint as the turnoff point. While a fraction of the clusters with such an EHB have an Harris HB type = 0, further clusters can be considered as owning EHBs. If one includes these clusters too, our candidates set has $N_{\text{EHB}} = 4$ and

$P(N_{\text{EHB}} \geq 4) \simeq 0.046$ (see Fig. 8, dashed histogram), consequently the confidence level rises to ~ 95 percent.

It is worth mentioning that the two candidates clusters considered not to possess an EHB in this analysis, show significant peculiarities in their HB. In particular, NGC 6388 shows an over-luminous blue HB (Rich et al. 1997; Raimondo et al. 2002; Catelan et al. 2006) and, similarly to what observed in M54 (Rosenberg, Recio-Blanco & García-Marín 2004), a blue HB extending anomalously beyond the theoretical zero-age HB (Busso, Piotto & Cassisi 2004).

It can be noticed that in the whole NG06 sample, there are 7 non-candidates clusters that possess EHB. This suggests that there might be other mechanisms – not related to the interaction with IMBHs – at work for the formation of EHB stars. However, 4 of those clusters are highly concentrated ($c > 2.4$) or core-collapsed. This confirms that, whatever the formation mechanism is, this is favoured by an highly density environment (Fusi Pecci et al. 1993; Buonanno et al. 1997).

Nevertheless, the presence of such an environment at the present time is not a sufficient condition for the formation of an IMBH, which is closely linked to the *initial* central density instead. Gravitational oscillations and collapse may have changed rapidly the former dynamical state, thus erasing the link with the initial environment. All this could explain the rather weak correlation found by Recio-Blanco et al. (2006) between T_{effHB} and the collisional parameter they defined on the basis of the present dynamical conditions. Furthermore, the velocity dispersion used in the definition could be not representative of the higher actual value in the inner (not resolved) cusp region.

However, there are other alternative explanations for the presence of blue subdwarfs, which are not based upon tidal stripping (see, e.g., Soker & Harpaz 2007; Catelan 2007, section 7.4).

6 CONCLUSIONS

In this paper, the multimass isotropic and spherical King model has been extended to include the Bahcall & Wolf (1976) distribution function in the central region, so as to account for the presence of a central intermediate-mass black hole (IMBH). This self-consistent model gen-

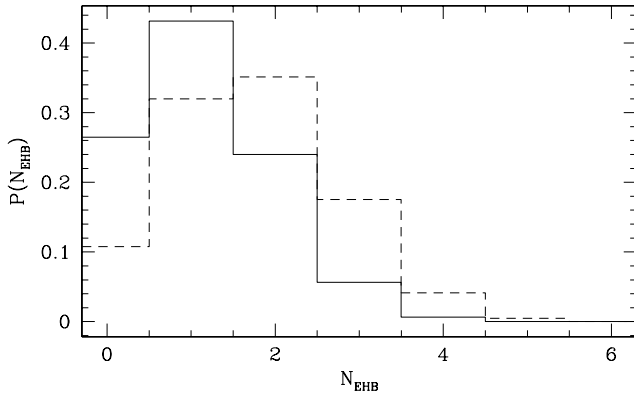


Figure 8. Probability distribution of finding N_{EHB} clusters having an extended blue tail, in a subset of 6 clusters randomly chosen from the NG06 set. The solid line histogram refers only to clusters with HB type = 0, while in the dashed one those having $\log(T_{\text{effHB}}) > 4.3$ are also taken into account. Our candidates clusters subset has $N_{\text{EHB}} = 3$ in the former case and = 4 in the latter.

erates surface brightness profiles that show a power-law behaviour around the centre and a core-like profile outwards. This latter is similar to a King profile with concentration $c < 2$, though slightly steeper in the core region. The following features are particularly relevant:

- (i) c decreases monotonically with the IMBH mass M_{\bullet} .
- (ii) IMBHs with $10^{-3}M \lesssim M_{\bullet} \lesssim 10^{-2}M$, with M the cluster mass, are compatible only with non-collapsed distributions ($c \lesssim 2$)
- (iii) the core surface brightness profiles exhibit a logarithmic slope $s \leq 0.25$ for reasonably low IMBH masses ($M_{\bullet} \lesssim 10^{-2}M$).

These features are basically in agreement with the results of collisional N -body simulations, which found that the IMBH causes a quick expansion of the a cluster core because of the enhanced collisional rate of exchange of kinetic energy between stars of different masses (Baumgardt et al. 2005) or between single stars and hard binaries in 3-body encounters occurring in the black hole vicinity (Trenti et al. 2007). Moreover, the radius below which the velocity dispersion profile is appreciably altered by the influence of the compact object turns out to be $\sim 3M_{\bullet}/M$ in units of the core radius. It is also seen that a completely cusp density profile (similar to, e.g., that of collapsed clusters) can be associated only to a black hole with a unrealistically high mass, even higher than that of the host cluster itself.

A grid of models is then generated to derive possible trends of the IMBH mass with the concentration and with the core logarithmic slope. It is found that, in general, $12s - 4.8 \lesssim \log(M_{\bullet}/M) \lesssim -1.1c - 0.69$. This mass range estimate is applied to a set of 38 galactic globular clusters recently re-analysed by Noyola & Gebhardt (2006) as well as to the case of G1 (in M31). It was found that 6 clusters in this sample probably host an IMBH, namely: NGC 2808, NGC 6388, M80, M13, M62 and M54. Among these, the M80 and M13 brightness profiles presented in Noyola & Gebhardt show the typical appearance of the

cuspy-core behaviour reproduced by the model. The scaling relations

$$M_{\bullet} \sim 0.02 \left(\frac{M}{M_{\odot}} \right)^{0.8} M_{\odot}, \quad (24)$$

$$M_{\bullet} \sim 100 \left(\frac{\sigma_{\text{obs}}}{\text{km s}^{-1}} \right)^{0.9} M_{\odot}, \quad (25)$$

are found to be followed by the candidates clusters.

Relation (24) is compatible to those found in larger scale systems, i.e. between the mass of super-massive BHs in galactic nuclei and that of the bulge (Magorrian et al. 1998), and the recently confirmed link between compact nuclei mass and the host spheroid mass in nucleated dwarf galaxies (Côté et al. 2006; Wehner & Harris 2006). None the less, relation (25) is significantly different for the analogous relation ascertained in galaxies (Ferrarese & Merritt 2000), but the discrepancy can be understood by noting that the scaling law between the total mass and the central velocity dispersion for galaxies is very different from that of globular clusters.

Unfortunately, the uncertainties on the mass range estimates are in many cases rather large and, as a consequence, the presence of IMBHs on other clusters cannot be completely ruled out. They are mainly due to the uncertainties in the central observed projected velocity dispersion, and in the logarithmic slope measures. For this reason, we plan to carry out individual studies on a representative cluster subset in the Noyola & Gebhardt (2006) sample, to infer the IMBH mass directly from the best parametric fit of their brightness profiles.

Nevertheless, this preliminary and ‘collective’ approach, permits to achieve an intriguing result: the presence of an extreme blue horizontal branch – determined according both to the Harris (1996) HB type index and to the maximum effective temperature of HB stars – is associated to the presence of the IMBH at a statistically significant level of confidence (> 90 percent). Such a correlation is not surprising when one takes into account the high stellar density in the inner cusp region and the relatively high ratio between M_{\bullet} and the single stellar mass, in calculating the rate of tidal stripping event in giants-IMBH close encounters.

This firmly suggests that the mass of the IMBH could be one of the ‘hidden’ parameters that are being searched for to explain the strong variability of HB morphology in clusters with the same metallicity (the so-called ‘2nd parameter’ problem). For instance, the presence of a central IMBH could explain why extreme HB stars are observed in M13 and NGC 6388, but not in M3 and 47 Tuc where such an object should be absent according to our analysis.

ACKNOWLEDGMENTS

The author would like to thank E. Brocato, G. Raimondo, A. Sills, G. Piotto and W.E. Harris for their helpful suggestions and discussion about extreme HB stars and morphology indicators. The author’s acknowledgments go also to M. Freitag for his valuable comments, as well as

to all the staff at the Osservatorio Astronomico di Teramo for the kind hospitality and the friendly atmosphere enjoyed during his stay.

REFERENCES

- Alexander T., 1999, *ApJ*, 527, 835
 Alexander T., 2005, *Phys. Rep.*, 419, 65
 Amaro-Seoane P., Freitag M., Spurzem R., 2004, *MNRAS*, 352, 655
 Bahcall J.N., Wolf R.A., 1976, *ApJ*, 209, 214
 Bahcall J.N., Wolf R.A., 1977, *ApJ*, 216, 883
 Baumgardt H., Hut P., Makino J., McMillan S., Portegies Zwart S., 2003a, *ApJ* 582, L21
 Baumgardt H., Makino J., Hut P., McMillan S., Portegies Zwart S., 2003b, *ApJ* 589, L25
 Baumgardt H., Makino J., Ebisuzaki T., 2004a, *ApJ*, 613, 1133
 Baumgardt H., Makino J., Ebisuzaki T., 2004b, *ApJ*, 613, 1143
 Baumgardt H., Makino J., Hut P., 2005, *ApJ*, 620, 238
 Baumgardt H., Hopman C., Portegies Zwart S., Makino J., 2006, *MNRAS*, 372, 467
 Binney J.J., Tremaine S., 1987, *Galactic Dynamics*. Princeton Univ. Press, Princeton, NJ
 Buonanno R., Corsi C. E., Bellazzini M., Ferraro F. R., Fusi Pecci F., 1997, *AJ*, 113, 706
 Busso G., Piotto G., Cassisi S., 2004, *Mem. Soc. Astron. It.*, 75, 46
 Capuzzo Dolcetta R., Leccese L., Merritt D., Vicari A., 2007, submitted to *ApJ* (astro-ph/0611205)
 Catelan M., 2007, in Valls Gabaud D., Chavez M., eds, *Resolved Stellar Populations*, ASP Conf. Series, in press. ASP, San Francisco (astro-ph/0507464)
 Catelan M. et al., 2006, *ApJ*, 651, L133
 Cohn H., Kulsrud R.M., 1978, *ApJ*, 226, 1087
 Colpi M., Devecchi B., Mapelli M., Patruno A., Possenti A., 2005, in *Interacting Binaries: Accretion, Evolution, and Outcomes*. AIP Conf. Proc., Vol. 797. American Inst. of Phys., p. 205 (astro-ph/0504198).
 Côté P., Welch D.L., Fischer P., Gebhardt K., 1995, *ApJ*, 454, 788
 Côté P. et al., 2006, *ApJS*, 165, 57
 Da Costa G. S., Freeman K. C., 1976, *ApJ*, 206, 128
 Dickens R.J. 1972, *MNRAS*, 157, 281
 Djorgovski S., 1993, in Meylan G., Djorgovski S., eds, *Structure and Dynamics of Globular Clusters*. ASP Conf. Ser. Vol. 50. Astron. Soc. Pac., San Francisco, p. 373
 Djorgovski S., Meylan G., 1994, *AJ*, 108, 1292
 Dubath P., Meylan G., Mayor M., 1997, *A&A*, 324, 505
 Fabbiano G., 2006, *ARA&A*, 44, 323
 Ferrarese L., Ford H., 2005, *Space Sci. Rev.*, 116, 523
 Ferrarese L., Merritt D., 2000, *ApJ*, 539, L9
 Ferraro F. R., Possenti A., Sabbi E., D'Amico N., 2003, *ApJ*, 596, L211
 Frank J., Rees M. J., 1976, *MNRAS*, 176, 633
 Freitag M., Benz W., 2002, *A&A*, 394, 345
 Freitag M., Amaro-Seoane P., Kalogera V., 2006a, *ApJ*, 649, 91
 Freitag M., Gürkan M.A., Rasio F.A., 2006b, *MNRAS*, 368, 141
 Fusi Pecci F., Ferraro F.R., Bellazzini M., Djorgovski S., Piotto G., Buonanno R., 1993, *AJ*, 105, 1145
 Gebhardt K., Rich R. M., Ho L. C., 2002, *ApJ*, 578, L41
 Gebhardt K., Rich R.M., Ho L.C., 2005, *ApJ*, 634, 1093
 Gerssen J., 2004, *AN*, 325, 84
 Gerssen J., van der Marel R.P., Gebhardt K., Guhathakurta P., Peterson R.C. Pryor C., 2002, *AJ*, 124, 3270
 Gerssen J., van der Marel R.P., Gebhardt K., Guhathakurta P., Peterson R.C. Pryor C., 2003, *AJ*, 125, 376
 Gunn J.E., Griffin R.F., 1979, *AJ*, 84, 752
 Gürkan M.A., Freitag M., Rasio , 2004, *ApJ*, 604, 632
 Harris W.E., 1996, *AJ*, 112, 1487
 Heggie D., Hut P., 2003, *The Gravitational Million-Body Problem: A Multidisciplinary Approach to Star Cluster Dynamics*. Cambridge University Press, Cambridge, NY.
 Hopman C., Alexander T., 2006, *ApJ*, 645, L133
 Jones B., 1970, *AJ*, 75, 563
 King I.R., 1966, *AJ*, 71, 64
 Kormendy, J., 2004, in Ho L. C., ed., *Carnegie Observ. Astroph. Ser. Vol. 1, Coevolution of Black Holes and Galaxies*. Cambridge Univ. Press, Cambridge, p. 1
 Lightman A.P., Shapiro S.L., 1977, *ApJ*, 211, 244
 Madau P., Rees M.J., 2001, *ApJ*, 551, L27
 Magorrian J. et al., 1998, *AJ*, 115, 2285
 McLaughlin D. E., et al. 2006, *ApJS*, 166, 249
 McNamara B.J., Harrison T.E., Anderson J., 2003, *ApJ*, 595, 187
 Meylan G., Heggie D.C., 1997, *A&AR*, 8, 1
 Meylan G., Sarajedini A., Jablonka P., Djorgovski S.G., Bridges T., Rich R.M., 2001, *AJ*, 123, 830
 Merritt D., 2004, in Ho L. C., ed., *Carnegie Observ. Astroph. Ser. Vol. 1, Coevolution of Black Holes and Galaxies*. Cambridge Univ. Press, Cambridge, p. 263 (astro-ph/0301257)
 Milone A.P., Villanova S., Bedin L.R., Piotto G., Carraro G., Anderson J., King I.R., Zaggia S., 2006, *A&A*, 456, 517
 Miocchi P., 2006, *MNRAS*, 366, 227
 Moehler S., 2001, *PASP*, 113, 1162
 Murphy B.W., Cohn H.N., Durisen R.H., 1991, *ApJ*, 370, 60
 Noyola E., Gebhardt K., 2006, *AJ*, 132, 447
 Noyola E., Gebhardt K., Bergmann M., 2007, submitted to *ApJ*
 Peebles P. J. E., 1972, *ApJ*, 178, 371
 Piotto G. et al. 2002, *A&A*, 391, 945
 Portegies Zwart S. F., Baumgardt H., Makino J., McMillan S.L., Hut P., 2004, *Nat*, 428, 724.
 Press W.H., Teukolsky S.A., Vetterling W.T., Flannery B.P., 1988, *Numerical Recipes in C: the Art of Scientific Computing*. Cambridge Univ. Press, Cambridge, NY
 Preto M., Merritt D., Spurzem R., 2004, *ApJ*, 613, L109
 Pryor C., Meylan G., 1993, in Meylan G., Djorgovski S., eds, *Structure and Dynamics of Globular Clusters*. ASP Conf. Ser., Vol. 50. Astron. Soc. Pac., San Francisco, p.357

- Raimondo G., Castellani V., Cassisi S., Brocato E., Piotto G., 2002, *ApJ*, 569, 975
- Rasio F.A. et al., 2006, in van der Hucht K.A., ed., *Highlights of Astronomy Vol. 14, Proc. XXVIth IAU General Assembly* (astro-ph/0611615)
- Recio-Blanco A., Aparicio A., Piotto G., De Angeli F., Djorgovski S.G., 2006, *A&A*, 452, 875
- Rich R.M., Minniti D., Liebert J., 1993, *ApJ*, 406, 489
- Rich R.M. et al., 1997, *ApJ*, 484, L25
- Richstone D., 2004, in Ho L. C., ed., *Carnegie Observ. Astroph. Ser. Vol. 1, Coevolution of Black Holes and Galaxies*. Cambridge Univ. Press, Cambridge, p. 280
- Rosenberg A., Recio-Blanco A., García-Marín M., 2004, *ApJ*, 603, 135
- Schwarzschild M., 1979, *ApJ*, 232, 236
- Shapiro S.L., 1985, in Goodman J., Hut P., eds, *Proc. IAU Symp. 113, Dynamics of Star Clusters*. Reidel, Dordrecht, p. 373
- Shapiro S.L., Lightman A.P., 1976, *Nat*, 262, 743
- Soker N., Harpaz A., 2007, submitted to *ApJ* (astro-ph/0701528)
- Tremaine S., et al. 2002, *ApJ*, 574, 740
- Trenti M., 2006, submitted to *MNRAS Letters* (astro-ph/0612040)
- Trenti M., Ardi E., Mineshige S., Hut P., 2007, *MNRAS*, 374, 857
- van den Bosch R., de Zeeuw P.T., Gebhardt K., Noyola E., van de Ven G., 2006, *ApJ*, 641, 852
- van de Ven G., van den Bosch R. C. E., Verolme E. K., de Zeeuw P. T., 2006, *A&A*, 445, 513
- van der Marel R.P., 2004, in L. C. Ho, ed., *Carnegie Observ. Astroph. Ser. Vol. 1, Coevolution of Black Holes and Galaxies*. Cambridge Univ. Press, Cambridge, p. 37 (astro-ph/0302101)
- Wehner E.H., Harris W.E., 2006, *ApJ*, 644, L17

This paper has been typeset from a $\mathrm{T}_\mathrm{E}\mathrm{X}$ / $\mathrm{L}^{\mathrm{A}}\mathrm{T}_\mathrm{E}\mathrm{X}$ file prepared by the author.